NASA-TM-112913

AIAA 96-0903
Six Degree-of-Freedom Entry Dispersion Analysis for the METEOR Recovery Module

Prasun N. Desai
Robert D. Braun
Richard W. Powell
Walter C. Engelund
Paul V. Tartabini
NASA Langley Research Center
Hampton, VA

34th Aerospace Sciences Meeting & Exhibit
January 15-18, 1996 / Reno, NV

Six Degree-of-Freedom Entry Dispersion Analysis for the METEOR Recovery Module

Prasun N. Desai*
Robert D. Braun*
Richard W. Powell**
Walter C. Engelund*
Paul V. Tartabini*
NASA Langley Research Center
Hampton, VA 23681-0001

ABSTRACT

The present study performs a six degree-of-freedom entry dispersion analysis for the Multiple Experiment Transporter to Earth Orbit and Return (METEOR) mission. METEOR offered the capability of flying a recoverable science package in a microgravity environment. However, since the Recovery Module has no active control system, an accurate determination of the splashdown position is difficult because no opportunity exists to remove any errors. Hence, uncertainties in the initial conditions prior to deorbit burn initiation, during deorbit burn and exo-atmospheric coast phases, and during atmospheric flight impact the splashdown location. This investigation was undertaken to quantify the impact of the various exo-atmospheric and atmospheric uncertainties. Additionally, a Monte-Carlo analysis was performed to statistically assess the splashdown dispersion footprint caused by the multiple mission uncertainties. The Monte-Carlo analysis showed that a 3-σ splashdown dispersion footprint with axes of 43.3 nm (long), -33.5 nm (short), and 10.0 nm (crossrange) can be constructed. A 58% probability exists that the Recovery Module will overshoot the nominal splashdown site.

NOMENCLATURE

α angle-of-attack (angle between the velocity vector and vehicle's xy plane), deg
α_T total angle between the velocity vector and the vehicle's axis of symmetry, deg
β sideslip angle (angle between the velocity vector and vehicle's xz plane), deg
γ flight-path angle, deg

Aerospace Engineer, Space Systems and Concepts Division, Member AIAA
**Senior Research Engineer, Space Systems and Concepts Division, Member AIAA*

INTRODUCTION

The Multiple Experiment Transporter to Earth Orbit and Return (METEOR) mission was launched aboard the inaugural flight of the Conestoga launch vehicle in October 1995. METEOR was a commercial program partially funded by NASA and developed by EER, Systems Incorporated. It was formerly known as the COMmercial Experiment Transporter (COMET) with the goal of flying experiments to orbit in a microgravity environment and

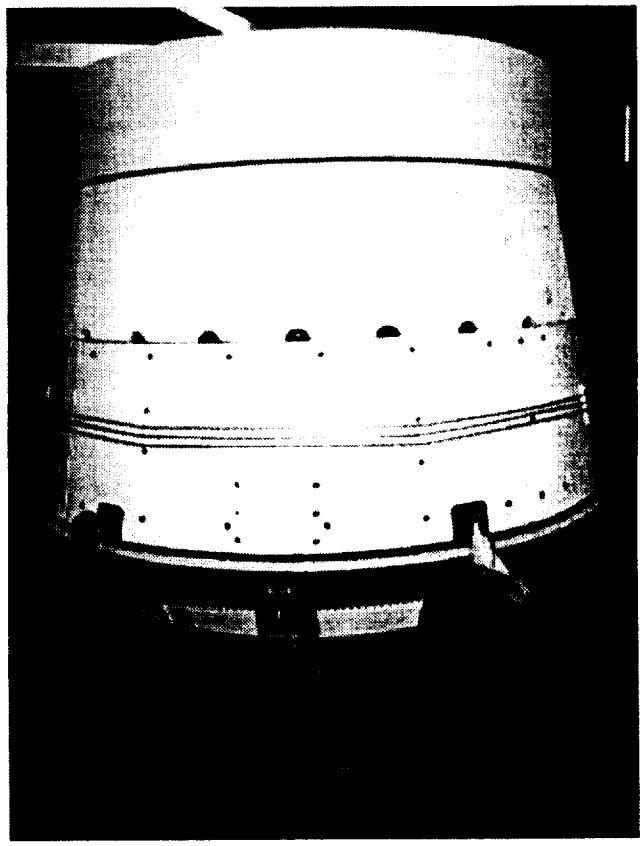

Fig. 1 Recovery module configuration.

then be able to recover them. The spacecraft consisted of a Service Module (SM) which remains in orbit and a Recovery Module (RM) which re-enters approximately 20 days after launch. The RM was originally designed by Space Industries, Inc., and an entry dispersion analysis of the mission was performed.[1,2,3,4] However, in 1995, EER took over the final development of the RM (Fig. 1), and modified the original mission (orbit altitude, spacecraft mass properties, and the nominal landing site). Also, the reliability of previous dispersion analysis was questioned due to a lack of credible aerodynamic data for the RM.[5] As a result, a six degree-of-freedom (DOF) entry dispersion analysis of the new mission scenario was necessitated.

The mission scenario is as follows (Fig. 2): METEOR was to be launched into approximately a 250 nm circular orbit from NASA Wallops having an orbital inclination of 40.5°. After approximately 20 days, the deorbit sequence begins. The attitude control system aboard the SM points the combined system to a specified attitude. With the use of a spin table, the RM is spun up to 73 rpm and separated from the SM. Since the RM has no active control system, the spin up provides stability to maintain its pointing attitude prior to performing the deorbit burn. Following a coast period (approximately one half orbit), the deorbit burn is performed to initiate the entry of the RM. Shortly before the atmospheric passage (approximately 500 kft), the RM is despun to a nominal 6.5 rpm by a yo-yo despin device. This despin maneuver is performed to reduce the gyroscopic stability of the RM;

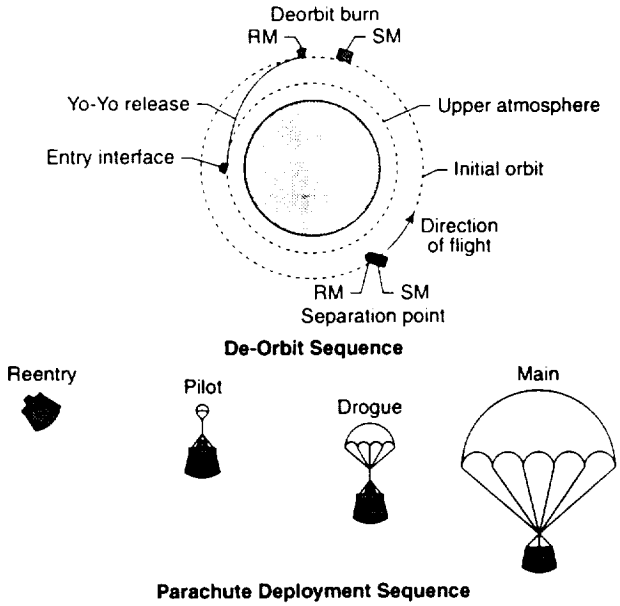

Fig.2 METEOR mission profile.

thus, allowing the vehicle's aerodynamic characteristics to reduce its angle-of-attack prior to peak heating. The vehicle aerodynamically decelerates from approximately 25,000 ft/s to subsonic speeds. At an altitude of 60 kft, a series of three parachute deployments begin to slow the RM before splashdown off the coast of Virginia. The RM is positively buoyant and will be picked up by a surface vessel so that the experiments can be recovered. Unfortunately, due to a failure aboard the Conestoga during ascent, the launch vehicle and METEOR were lost.

ANALYSIS

Aerodynamics

The aerodynamic database utilized in the flight simulation studies was derived from a combination of computational fluid dynamics calculations, wind tunnel, and engineering code results. Since the flight traverses different flow regimes (rarefied, transitional, continuum), a range of solution methods were required to estimate the aerodynamics of the RM. Free molecule models were employed at altitude above 394 kft (120 km); Direct Simulation Monte Carlo (DSMC) models[6] were used for altitudes between 295 kft (90 km) and 394 kft (120 km); and a Navier-Stokes solver[7] was applied at altitudes below 263 kft (80 km). The Navier-Stoke solutions were augmented with experimental data at Mach 6 and at Mach numbers between 1.60 and 2.85. Subsonic aerodynamic characteristics were obtained with a linearized potential flow solver. In the transition region between 263-295 kft (80-90 km), the aerodynamics are obtained through linear interpolation. The continuum aerodynamic characteristics of the METEOR Recovery Module are explained in detail in Ref. 8. Additionally, due to the RM's configuration similarity with the Mercury manned entry capsule, dynamic stability aerodynamics were estimated based on Mercury-capsule flight data.[9]

Six DOF Trajectory Simulation

The trajectory analysis was performed using the six and three DOF versions of the Program to Optimize Simulated Trajectories (POST)[10]. This program has been utilized previously in similar applications.[11,12] The six DOF version of this program was used to integrate the equations of motion from prior to the deorbit burn to parachute deployment. The three DOF program was then used from parachute deployment to splashdown. The six DOF simulation includes the Earth atmospheric (GRAM-95)[13] and gravitational models, vehicle aerodynamics, mass properties and propulsion mod-

els, SM separation, and yo-yo release/despin models. The yo-yo release/despin is modeled using the method developed by Etter and Shamey.[14] Their method models three-dimensional motion (i.e., precession and nutation), and allows for both center-of-gravity offsets and products of inertia. The three DOF simulation includes non-instantaneous parachute deployment models and the jettisoning of the RM's aft endcap. Since the RM has no active control system, no formal guidance and control strategy was utilized.

Numerous sources of uncertainty affect the METEOR flight model. One source for this uncertainty arises through system capability limitations (e.g., the attitude control system on the SM can only achieve the prescribed pointing direction to within a specified tolerance). A lack of knowledge concerning the flight-day density, pressure, and winds and the computational uncertainty of the aerodynamics analysis are also contributing sources of error. Furthermore, measurement limitations in the mass, moments of inertia, center-of-gravity, and thrust nozzle alignment will also result in uncertainties. In this analysis, an attempt was made to conservatively quantify and model the degree of uncertainty in each mission parameter.

Table 1. Exo-Atmospheric Mission Uncertainties

Mass Properties		
Mass	±2 lb	
cg position along spin axis	±0.25 in. (2)	
cg position off spin axis	±0.25 in. (2)	
Major moment of inertia (I_{xx}, I_{yy}, I_{zz})	±1%	
Cross products of inertia (I_{xy}, I_{xz}, I_{yz})	±0.15 slug-ft^2	
Post-Separation State Vector		
Radial position	±656 ft	
In-track position	±8202 ft	
Cross-track position	±1312 ft	
Radial velocity	±0.66 ft/s	
In-track velocity	±1.08 ft/s	
Cross-track velocity	±1.12 ft/s	
Pitch/yaw attitude	±1.5°	} correlated
Pitch/yaw rate	±0.3 deg/sec	} correlated
Roll rate	±22 deg/sec	
Solid-Rocket Event		
Burn initiation time	±0.5 s	
Rocket motor temperature	±10°F	
Impulse	±0.5%	
Thrust vector cant angle	±0.45°	
Yo-Yo Event		
Despin initiation time	±0.5 s	
Terminal roll rate	±3.75 rpm	
Separation		
Spring induced velocity	0.226 ft/sec	

Table 2. Atmospheric Mission Uncertainties

Atmospheric Flight	
Transitional aerodynamics, C_A	±5%
C_N, C_Y	±0.06
C_m, C_n	±0.01
Continuum aerodynamics above Mach 10, C_A	±2%
C_N, C_Y	±0.05
C_m, C_n	±0.003
Continuum aerodynamics below Mach 5, C_A	±10%
C_N, C_Y	±0.05
C_m, C_n	±0.005
Dynamic stability coefficients, C_{mq}, C_{nr}	±50%
Pressure, GRAM-95 model	3-σ scale factors (3)
Density, GRAM-95 model	3-σ scale factors (3)
Winds, GRAM-95 model	3-σ scale factors (3, each component)
Parachute deployment altitude (pilot/drogue)	±1000 ft
Parachute deployment altitude (main)	±500 ft
Parachute aerodynamics, C_A	±20%

For this mission, 57 potential uncertainties were identified. These uncertainties are grouped into two categories (exo-atmospheric and atmospheric) and are listed in Tables 1 and 2, respectively, along with the corresponding 3-σ variances. As seen, a few of the uncertainties have multiple entries (in parentheses) to account for variations at different mission phases. For example, in Table 1, there are two center-of-gravity off-axis position uncertainties (denoted by a 2 in the parentheses). The first is applied prior to the deorbit burn to account for center-of-gravity measurement errors before launch, while the second is applied after the deorbit burn to account for unsymmetrical burning. For modeling the atmospheric properties (pressure, density, and winds: North-South, East-West, and vertical), three uncertainties are used to provide a variation with altitude. Note the 3-σ uncertainties listed in Tables 1 and 2 are estimates based on judgments of various experts in the field, and are not based on statistical analysis (see Acknowledgments).

RESULTS AND DISCUSSION

Nominal Mission

Figures 3a and 3b show the groundtrack of the nominal entry trajectory, where the major mission events are highlighted. The splashdown point is at a latitude of 36.93° N and a longitude of 73.87° W, which is about 95 nm off the coast of Virginia. Table 3 lists the nominal set of mass properties of the RM. Note, in Table 3, the RM has a small nominal engine cant angle value; thus, the nominal engine thrust vector does not go through the center-of-gravity (cg) of the vehicle.[15]

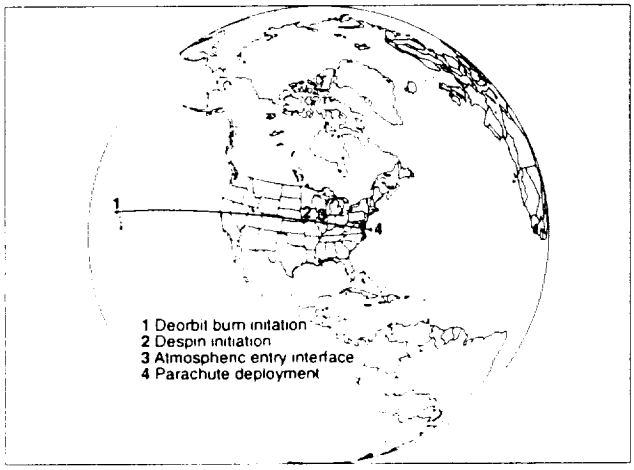

(a) Global view.

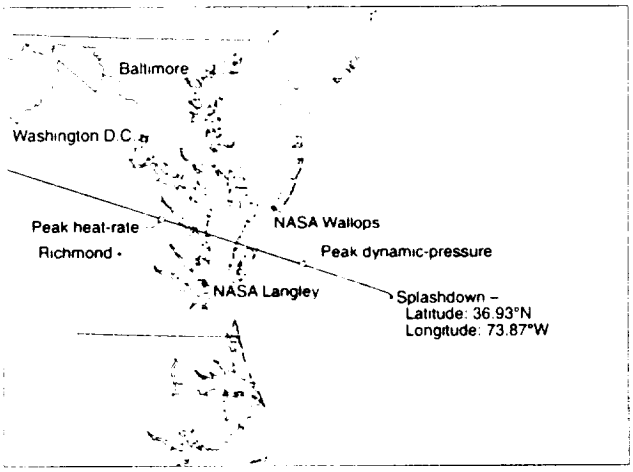

(b) Terminal mission segment.

Fig. 3 Nominal mission groundtrack.

Table 3. Nominal Mass Properties of the Recovery Module

	Deorbit	Entry
Weight, lb	763.0	686.5
Center-of gravity, ft:		
Along spin axis (x-direction, from nose)	1.713	1.597
Off spin axis (y-direction)	-0.00161	-0.00161
Off spin axis (z-direction)	-0.00213	-0.00213
I_{xx}, slug-ft^2	46.40	46.23
I_{yy}, slug-ft^2	41.58	40.43
I_{zz}, slug-ft^2	40.47	39.15
I_{xy}, slug-ft^2	0.0191	0.019
I_{xz}, slug-ft^2	-0.0191	-0.0185
I_{zz}, slug-ft^2	0.027	0.0261
Engine cant angle, deg	0.22	0.22

Figures 4 and 5 show flight characteristics of the nominal entry profile. The vehicle aerodynamically decelerates from approximately 25,000 ft/s to subsonic speed. During this time, the vehicle's aerodynamic stability reduces the total angle-of-attack to a moderate value (near 15°), as shown in Fig. 5. Peak heating occurs near Mach 21 with an angle of attack between 15° and 20°. The nominal attitude motion may be described by the superposition of two cycles, one in α, the other in β, each of which is centered on 0°. Because the two cycles are out of phase, the total angle-of-attack, α_T (defined as the angle between the velocity vector and the vehicle's axis of symmetry), never reaches 0°. As shown in Figs. 4a and 5, a majority of the vehicle's attitude decrease occurs while flying in the transitional aerodynamic regime. This is the reason for the computational investment in the DSMC flowfield solutions. Without these computational solutions, the validity of this diminishing attitude motion (which is critical to mission success) would be questionable.

Also shown in Fig. 5 is an increase in the total angle-of-attack towards the end of the entry. This behavior is an outcome of the sharp decrease in flight-path angle observed at the end of the entry (Fig. 4a). This area is also the region of flight (lower velocities) in which dynamic-stability issues begin to dominate. If the vehicle was dynamically unstable, the RM would not be able to follow this flight-path angle drop and extremely high angles-of-attack would result. In the extreme case, a tumbling motion could result prior to parachute deployment. However, because the vehicle is dynamically

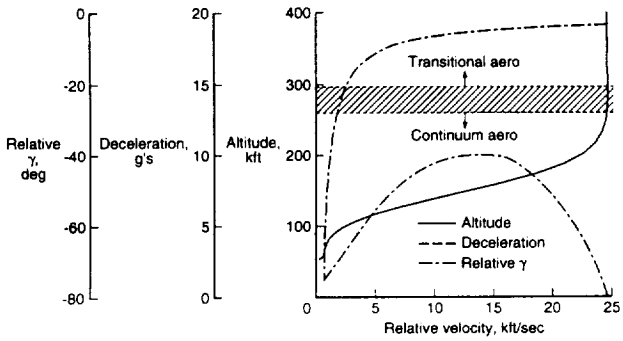

(a) Entry sequence.

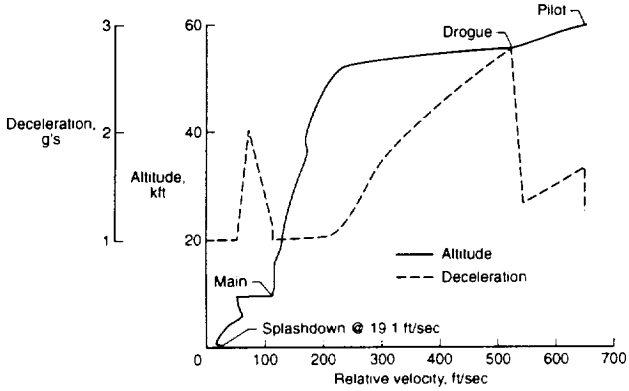

(b) Parachute deployment sequence.

Fig. 4 Nominal mission profile.

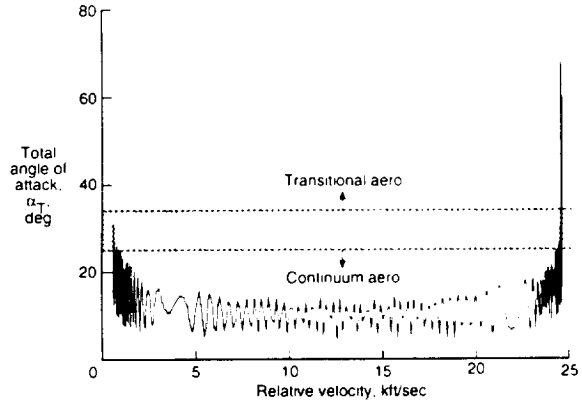

Fig. 5 Nominal mission attitude profile.

stable at all but the smallest total angles-of-attack, a tumbling motion does not occur. Rather, the vehicle's dynamic-stability helps to minimize the effect of the flight-path angle variations. Consequently, the total angle-of-attack at parachute deployment for the nominal mission is on the order of 25°.

Beginning at an altitude of 60 kft (approximately Mach 0.8), a series of three parachutes are deployed which slow the RM down to approximately 19 ft/s prior to splashdown. Each of these parachute deployments is evident in Fig. 4b.

Independent Uncertainty Effects

To identify the mission uncertainties which have the greatest impact on the splashdown dispersion, each mission uncertainty was varied independently at its respective ±3-σ value. Figure 6 shows the resulting splashdown range dispersions for the largest contributors to the splashdown dispersion size. Mission uncertainties not depicted in Fig. 6 had splashdown dispersions less than 2 nm.

As can be seen from Fig. 6, the mission parameters have a varying effect on the splashdown dispersion. The dispersions can be grouped into three categories: major (mission uncertainties 1-2), moderate (mission uncertainties 3-9), and small (mission uncertainties 10-20). The first group responsible for the largest dispersions, on the order of 25-30 nm, only include the exo-atmospheric uncertainties. These uncertainties produce the largest dispersion because they alter the deorbit burn direction. For example, a center-of-gravity offset (mission uncertainty 1) causes a change in the location of where the thrust vector is applied from the nominal mission; producing the large splashdown dispersion. The second group of uncertainties produce dispersion on the order of 10-20 nm. Included in this group are several exo-atmospheric effects (specific impulse, rocket-nozzle cant-angle, and the initial weight uncertainties) and several atmospheric effects (mid-altitude density and low-altitude

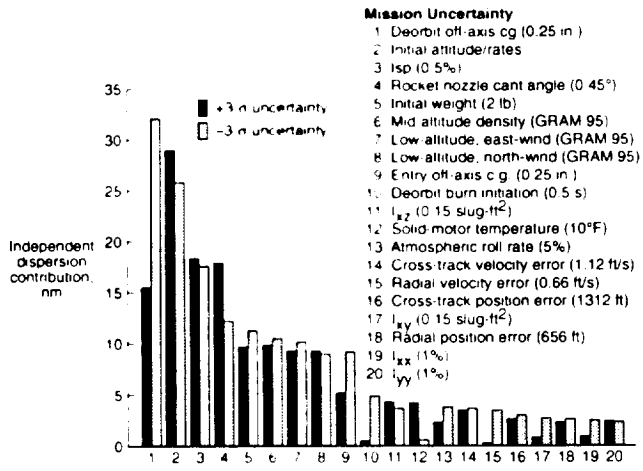

Fig. 6 Significant contributors to the total splashdown range dispersion (3-σ variance shown in parenthesis)..

horizontal and vertical winds uncertainties). The third group of uncertainties produce dispersions less than 5 nm. These uncertainties include those resulting from initial state-vector errors, moments of inertia misprediction, variation in the atmospheric roll rate, and propulsion system unknowns (temperature and burn initiation time).

As seen in Fig. 6, some of the mission uncertainties have a drastic difference in the dispersion between the +3-σ and -3-σ values (mission uncertainties 1, 9, 10, 12, 15, 17, 19). This outcome is due to the RM having a non-zero nominal engine cant angle value. Consequently, when the ±3-σ values are applied (for one of these mission uncertainties), one bound heightens the effect of the engine cant angle, while the other boundary value counteracts this effect. If there was no nominal engine cant angle, the resulting dispersions caused by the ±3-σ uncertainties would be more symmetric.

Table 4. Major Contributors to Total Splashdown Range Dispersion

	Dispersion with +3-σ Uncertainty (nm)	Dispersion with -3-σ Uncertainty (nm)
1. Deorbit off-axis cg (0.25 in.)	15.5	32.1
2. Initial attitudes/rates	29.0	25.8
3. Isp (0.5%)	18.4	17.6
4. Rocket nozzle cant angle (0.45°)	17.9	12.2
5. Initial weight (2 lb)	9.7	11.3
6. Mid-altitude density (GRAM 95)	9.9	10.5
7. Low-altitude, east-wind (GRAM 95)	9.3	10.2
8. Low-altitude, north-wind (GRAM 95)	9.3	9.0
9. Entry off-axis c.g. (0.25 in.)	5.2	9.2
10. Deorbit burn initiation (0.5 sec)	0.5	4.9
11. I_{xz} (0.15 slug-ft^2)	4.3	3.7
12. Solid-motor temperature (10°F)	4.2	0.6
13. Atmospheric roll rate (5%)	2.3	3.8
14. Cross-track velocity error (1.12 ft/s)	3.5	3.7
15. Radial velocity error (0.66 ft/s)	0.3	3.5
16. Cross-track position error (1312 ft)	2.6	3.0
17. I_{xy} (0.15 slug-ft^2)	0.8	2.7
18. Radial position error (656 ft)	2.3	2.6
19. I_{xx} (1%)	0.9	2.5
20. I_{yy} (1%)	2.4	2.3
Approximate 3-σ Total	**53.6**	**61.0**

All other contributors < 2 nm

The one-variable-at-a-time results are summarized in Table 4. Note that relative to the exo-atmospheric unknowns, the atmospheric uncertainties do not have a major impact on the splashdown dispersion. Furthermore, the aerodynamic uncertainty associated with the mission has a minimal impact on the splashdown dispersion size. Computing the L_2 norm of these one-variable-at-a-time results, an upper-bound on the resulting 3-σ range dispersion from the Monte-Carlo analysis of no more than 50-60 nm is expected.

Multiple Uncertainty Effects

To determine the effects of multiple uncertainties occurring during the entry, a Monte-Carlo analysis is performed. Over 3500 random trajectories were simulated to assure a gaussian distribution.

For some Monte-Carlo cases, a high amplitude oscillatory behavior in the total angle-of-attack near atmospheric interface was observed. As a result, for this vehicle, the total angle-of-attack at atmospheric interface is difficult to pinpoint. This behavior can be observed in Fig. 7 (starting at an altitude of 500 kft) for a particular Monte Carlo case, where the total angle-of-attack at atmospheric interface can be anywhere between 60 -120 . This phenomenon is a consequence

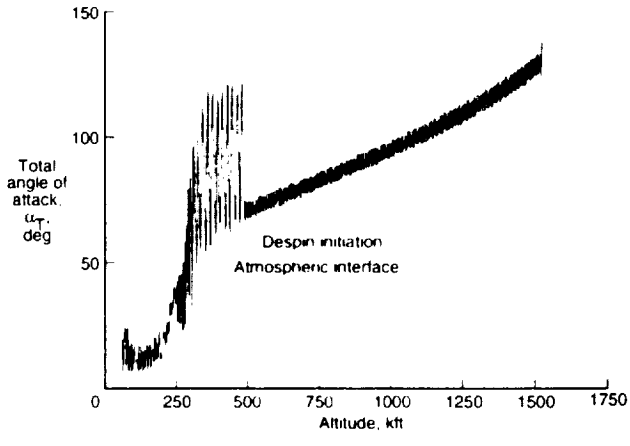

Fig. 7 Oscillatory motion in total angle-of-attack.

of high pitch and yaw energies which are produced during the deorbit burn due to the thrust vector misalignment, cant angle, and the center-of-gravity uncertainty. During the early stages of the mission, these pitch and yaw energies are suppressed by the high roll rate (73 rpm) of the vehicle which provides inertial stability. With the RM despun to 6 rpm, roll stability is reduced and the pitch and yaw rates dominate the rotational motion. This behavior is not present in the nominal mission (Fig. 5). However, a slight perturbation in one or a combination of the mission uncertainties can lead to this oscillatory motion. Approximately, 25% of the Monte-Carlo cases displayed this behavior.

As a result of the oscillatory motion, the mean oscillatory value of the total angle-of-attack at atmospheric interface is used to express the true attitude of the RM. Figures 8-10 show the distribution of the total angle-of-attack at atmospheric interface, peak heating, and parachute deployment. At atmospheric interface, the mean of the mean total angle-of-attack is 66.8° with an oscillation amplitude of 17.2°. At peak heating and parachute deployment, the mean total angle-of-attack is 20.6° and 51.2°, respectively. The maximum total angle-of-attack at each of these events can be significantly higher than these mean values. Maximum values of 176.6° (111.4° plus a 65.2° oscillation) at atmospheric interface, 56.7° at peak heating, and 170.5° at parachute deployment were obtained. Table 5 summarizes these results. Note, the heatshield design limit on the total angle-of-attack at atmospheric interface of 75° is violated in some cases. However, since the frequency of the oscillatory motion is high, the heating levels on the side and aft end of the RM (for these high total angle-of-attack cases) were determined to be acceptable.[16,17] In addition, the reliability of the aerodynamic

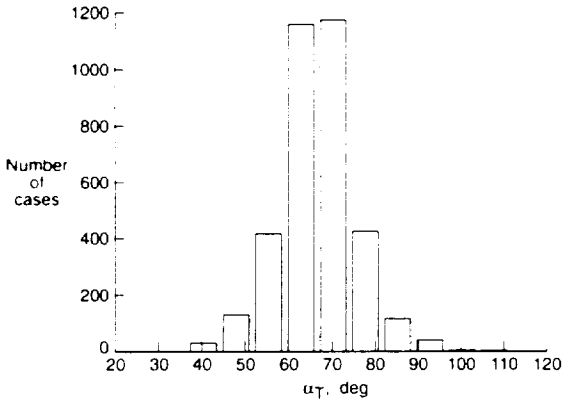

Fig. 8 Distribution of the mean total angle-of-attack at atmospheric interface resulting from over 3500 Monte-Carlo simulation cases.

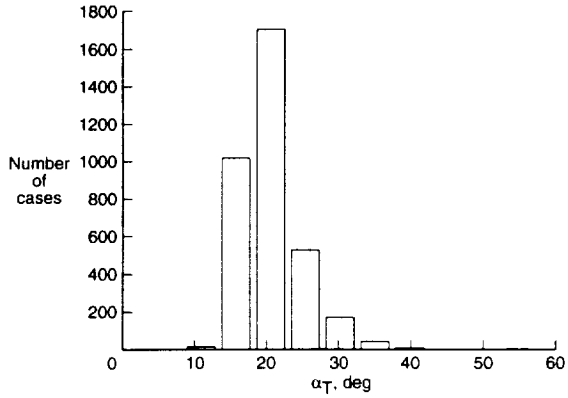

Fig. 9 Distribution of the total angle-of-attack at peak heating resulting from over 3500 Monte-Carlo simulation cases.

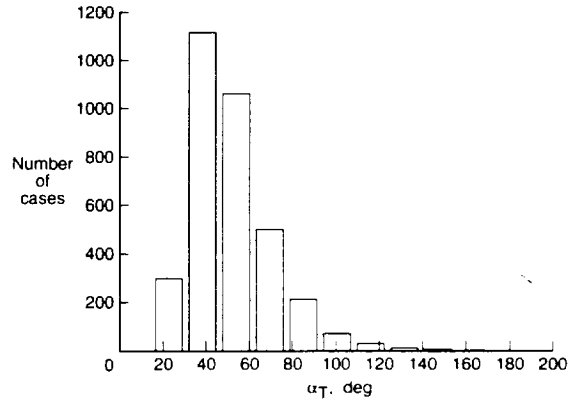

Fig. 10 Distribution of the total angle-of-attack at parachute deployment resulting from over 3500 Monte-Carlo simulation cases.

database for high altitudes and angle-of-attacks greater than 145° is questionable, because these conditions exceed the limit of the database. Approximately, 0.3% of the Monte-Carlo cases had total angle-of-attacks greater than 145.0°.

Figures 11 and 12 show the downrange and crossrange distribution at splashdown, respectively. The minimum downrange is -43.8 nm (short) from the nominal splashdown point, while the maximum downrange is 67.0 nm (long). The maximum crossrange obtained is 11.5 nm. A 3-σ dispersion footprint with axes of 43.3 nm (long), -33.5 nm (short), and 10.0 nm (crossrange) can be constructed. Within the assumptions of the present analysis, a 99.73% probability exists that the RM will splashdown within this 3-σ footprint. Table 5 summarizes these and other statistical results.

Table 5. Summary of Monte-Carlo Analysis

	Mean	Min	Max	3-σ
Mean atmospheric interface attitude, deg	66.8	36.6	111.4	26.2
Amplitude about mean atmospheric interface attitude, deg	17.2	1.6	65.2	28.7
Peak heating attitude, deg	20.6	8.5	56.7	12.8
Parachute deployment attitude, deg	51.4	14.9	170.5	56.7
Splashdown downrange, nm	2.6	-43.8	67.0	43.3 (long) -33.5 (short)
Splashdown crossrange, nm	-0.5	-11.5	10.9	10.0
Total splashdown range, nm	11.0	0.2	67.6	23.8
Splashdown latitude, deg	36.83	36.52	37.17	0.26
Splashdown longitude, deg	286.10	285.22	287.40	0.76

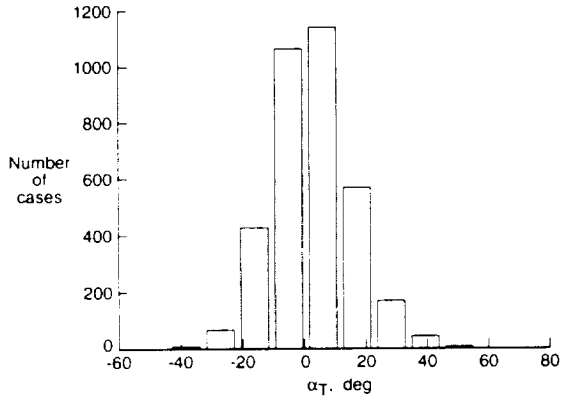

Fig. 11 Downrange at splashdown.

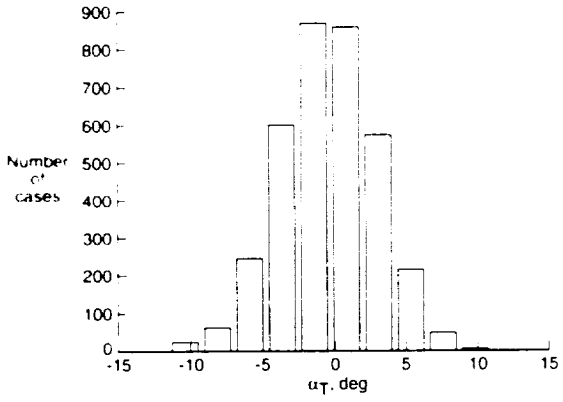

Fig. 12 Crossrange at splashdown.

Figures 13 and 14 show the atmospheric interface and splashdown locations for each of the cases. Note, the total downrange dispersion shown in these figures is similar. This outcome is due to the dominant effect which the exo-atmospheric uncertainties have upon downrange. While impacting downrange to some extent, the atmospheric uncertainties have a more pronounced effect on crossrange. Additionally, there is a slightly higher probability (58%) that the trajectory will splashdown long than short.

The present results predict a larger splashdown dispersion than previous METEOR entry dispersion analyses that were performed early in the program.[3,4] Table 6 summarizes the findings from Refs. 3 and 4. The splashdown predictions from the present analysis are approximately double that

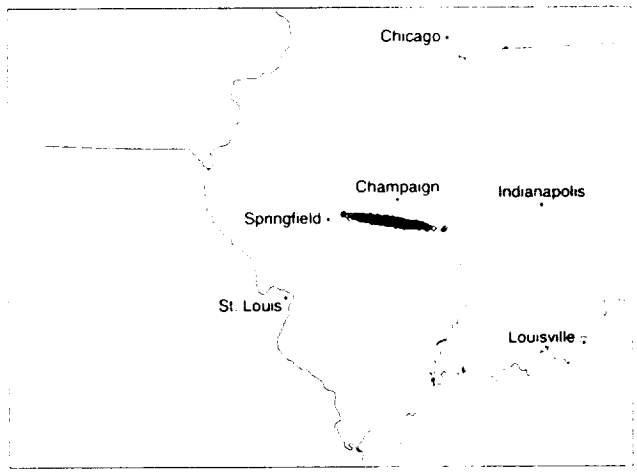

Fig. 13 Range dispersion at atmospheric interface resulting from over 3500 Monte-Carlo simulation cases.

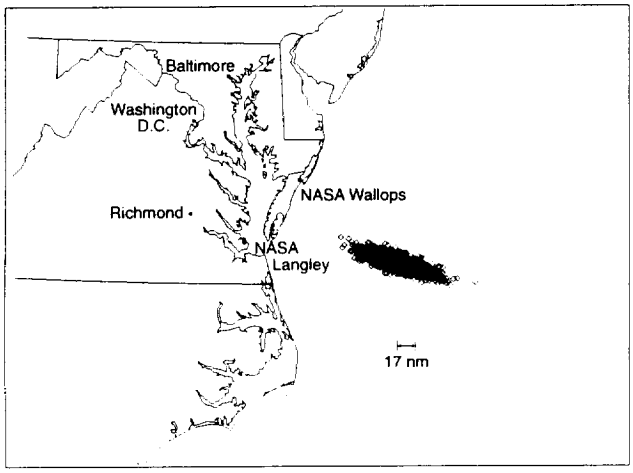

Fig. 14 Range dispersion at splashdown resulting from over 3500 Monte-Carlo simulation cases.

Table 6. Summary of Previous Entry Dispersion Analysis

Mission Uncertainty	Space Industry[3] Dispersion (nm)	Aerospace Corp.[4] Dispersion (nm)
One-At-A-Time Results		
Atmosphere (20%[3], 10%[4])	14.0	8.5
Isp (0.25%[3,4])	10.3	13.5
Ballistic coefficient (5.0 lb/ft^2 [4])	NA	9.6
Drag coefficient (10%[3])	6.2	NA
Atmospheric roll rate (3.75 rpm[3])	6.3	0
Initial attitude (0.7 deg[3], 0.5 deg[4])	6.2	0.8
Initial weight (1.2 lb[3])	6.0	0
State vector	5.9	3.2
Winds	4.2	0
Deorbit burn initiation (0.65 s[3], 1.0 s[4])	2.4	0.2
Parachutes	2.0	0
Solid-motor temperature (5°F[3])	2.0	0
Thrust cosine loss (1.5 deg[3])	1.0	0
Monte-Carlo Results		
Downrange, nm	22.4 (long)	17.0 (long)
	-22.4 (short)	-17.0 (short)
Crossrange, nm	3.8	2.9

of Refs. 3 and 4. The differences in these results can be attributed to many factors. The initial orbit altitude, target landing site, and mass properties of the RM have changed. More mission uncertainties are considered in the present analysis than in the previous studies. These additional uncertainties add to the overall dispersion. Additionally, the 3-σ variances selected in the present study are based on more conservative estimates (roughly twice that of the previous studies in some cases, e.g., Isp, solid-motor temperature, weight, and initial attitude/rates). Moreover, the aerodynamic characteristics of the RM are much better known due to the extensive computational and experimental investment. Overall, the present analysis produced a more conservative estimate of the splashdown dispersion.

SUMMARY

The present study performs a six degree-of-freedom entry dispersion analysis for the Multiple Experiment Transporter to Earth Orbit and Return (METEOR) Recovery Module. For this mission, 57 potential exo-atmospheric and atmospheric uncertainties were identified. From a one-variable-at-a-time uncertainty analysis, where each variable was set at its estimated $\pm$3-σ value, a center-of-gravity offset from the spin axis and initial attitude/rate uncertainties where shown to produce the greatest dispersions (each on the order of 30 nm). Uncertainties in specific impulse, engine cant angle, initial weight, mid-altitude density, and low-altitude winds produced dispersions on the order of 10-20 nm each. All other uncertainties produced dispersions less than 5 nm. From a Monte-Carlo analysis of over 3500 random, off-nominal trajectories, a 3-σ splashdown dispersion footprint with axes of 43.3 nm (long), -33.5 nm (short), and 10.0 nm (crossrange) was obtained. Within the assumptions of the present analysis, a 99.73% probability exists that the RM will splashdown within this 3-σ footprint. Additionally, there is a 58% probability that the Recovery Module will overshoot the nominal splashdown site. Furthermore, the present analysis predict a larger splashdown dispersion than previous METEOR entry dispersion analyses.

ACKNOWLEDGMENTS

The authors would like to thank Jack Levine of NASA Headquarters and Jim Hengle of EER Systems, Incorporated for the opportunity to participate in this flight program. Additionally, the assistance of personal from the Jet Propulsion Laboratory, the Aerospace Corporation, Kaman Sciences Corporation, Morton Thiokol, Ball Aerospace, EER Systems Incorporated, CTA Space Systems, NASA Goddard Space Flight Center, NASA Wallops Flight Facility, and NASA Langley Research Center in determining the exo-atmospheric and atmospheric 3-σ mission uncertainty values used in this analysis is also greatly appreciated.

REFERENCES

1. Hill, S.M, "Preliminary COMET Recovery Targeting and Dispersions," AIAA Paper 92-4659, 1992.

2. Hill, S.M and McCusker, T.J., "COMET Recovery System Flight Dynamics," AIAA Paper 93-3693, August 1993.

3. McCusker, T.J. and Hill, S.M., "Landing Dispersions for the Commercial Experiment Transporter Recovery System," AIAA Paper 93-3695, August 1993.

4. Summerset, T.K.; et al., "Comet Deorbit and Reentry Error Analysis," The Aerospace Corporation, Contract No. F04701-88-C-0089, August 1992.

5. Braun, R.D.; et al.: "Six-Degree-of-Freedom Aerodynamic Assessment and Monte-Carlo Dispersion Analysis for Reentry of the METEOR Capsule," Proposed NASA TM, June 1996.

6. Rault, D.F., "Aerodynamics of the Shuttle Orbiter at High Altitudes," Journal of Spacecraft and Rockets, Vol. 31, No. 6, Nov.-Dec. 1994.

7. Gnoffo, P.A., "Upwind-Biased, Point-Implicit, Relaxation Strategies for Viscous Hypersonic Flows," AIAA Paper 89-1972, June 1989.

8. Wood, W.A.; Gnoffo, P.A.; and Rault, D.F., "Aerothermodynamic Analysis of Commercial Experiment Transporter (COMET) Reentry Capsule," AIAA Paper 96-0316, Jan. 1996.

9. Bowman, J.S., "Dynamic Model Tests at Low Supersonic Speeds of Project Mercury Capsule Configurations With and Without Drogue Parachutes," NASA TM X-459, Feb. 1961.

10. Brauer, G.L.; Cornick, D.E.; and Stevenson R., "Capabilities and Applications of the Program to Optimize Simulated Trajectories (POST)," NASA CR-2770, Feb. 1977.

11. Powell, R.W.; Braun, R.D., "Six-Degree-of-Freedom Guidance and Control Analysis of Mars Aerocapture," *Journal of Guidance, Control, and Dynamics*, Vol. 16, No. 6, pp. 1038-1044, Nov.-Dec. 1993.

12. Braun, R.D.; Powell, R.W.; Engelund, W.C.; Gnoffo, P.A.; Weilmuenster, K.J.; Mitcheltree, R.A., "Six-Degree-of-Freedom Atmospheric Entry Analysis for the Mars Pathfinder Mission," AIAA Paper 95-0456, Jan. 1995.

13. Johnson, D.L.; Jeffries, W.R.; Yung, S.; and Justus, C.G., "Improved Global Reference Atmospheric Model (GRAM) Data Base," AIAA Paper 95-0545, Jan. 1995.

14. Etter, J.R. and Shamey, L.J., "Kane's Dynamical Equations and an Initial Value Problem for a Spacecraft Yo-Yo Despin System," AIAA Paper 91-2746, 1991.

15. Personal communication with Mark Daniel's, METEOR Mission Manager, EER Systems, Incorporated, Oct. 1995.

16. Personal communication with Jim Zimmer, Aerotherm Corporation, Oct. 1995.

17. Personal communication with Jim Hengle, Vice-President of Space Systems Group, EER Systems, Incorporated, Oct. 1995.